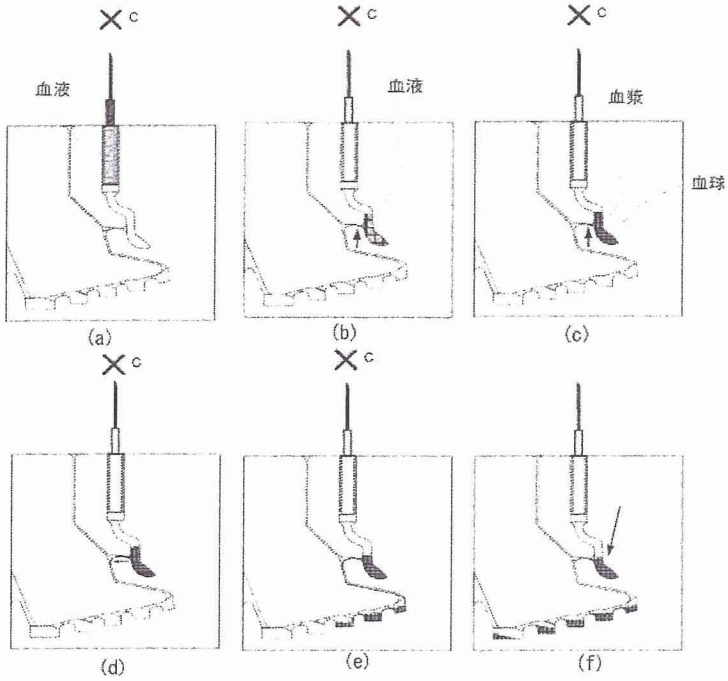

図 5　血球･血漿分離、血漿秤量遂行の様子

以上のような血球･血漿分離、血漿秤量機構の場合、最大回転数は R2 であり、これは細管流路を通過できる程度の遠心力が印加できる回転数でよく、また高い加速度は必要としないので、以前のチップの場合のように高性能のモーターは必要としない。

その他の以前のチップの問題点、第 1 の試液 A とだ 2 の試液 B をチップへと注入するタイミングは、同じく第 1 のチップ回転前と同一にできるよう、チップレイアウトを行い、またチップの厚みは試液収容槽や同秤量層の形状を改善することで、約 8mm まで低減（以前は約 13mm）した。以上のような改良を施したチップを図 6 に示すように作製し、評価を行った。

（倫理面への配慮）

本申請研究の初期特性確立への実施は物質･材料研究機構で行われる。本機構では人血の採取、採血具などについて外部の有識者を含む倫理委員会が設立されておりその厳格な規定に基づいて研究を進める。動物実験にあたっては、動物の愛護および管理に関する法律（昭和 48 年法律第 105 号）ならび実験動物の飼養及び保管等に関する法律（昭和 55 年総理府告示第 6 号）を遵守する。前臨床実験にあたっては、各研究機関のガイドラインに沿った計画を倫理委員会で検討、承認を得た後に、書面でのインフォームド･コンセントを確認する。

C. 研究結果

C.1 血球血漿分離と血漿秤量

まず、図 6 に示したチップの第 1 層に導入した血液を、血球と血漿に分離し、なおかつこの分離した血漿を 3 つに分割秤量することができるかどうかを確認した。図 7(i)に示すように、採血モジュールに約 6μℓの血液を静脈より採取して、これをチップに装着し、まず、チップを図中の回転軸 C を中心に 1500rpm で回転させ、採血モジュールから、分離流路へと血液を移動させる。このとき血液はキャピラリバルブ（細管流路）を通過できない（同図(ii)）。このまま 2 分間チップを回転

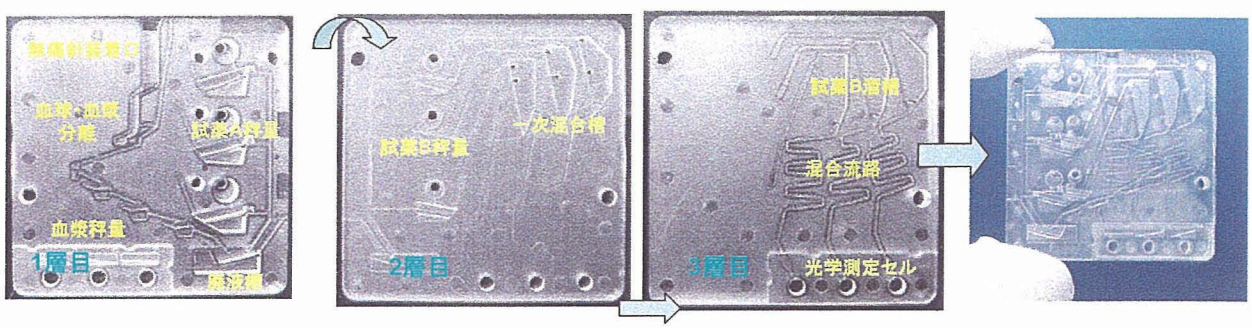

図 6　改良チップの構造。

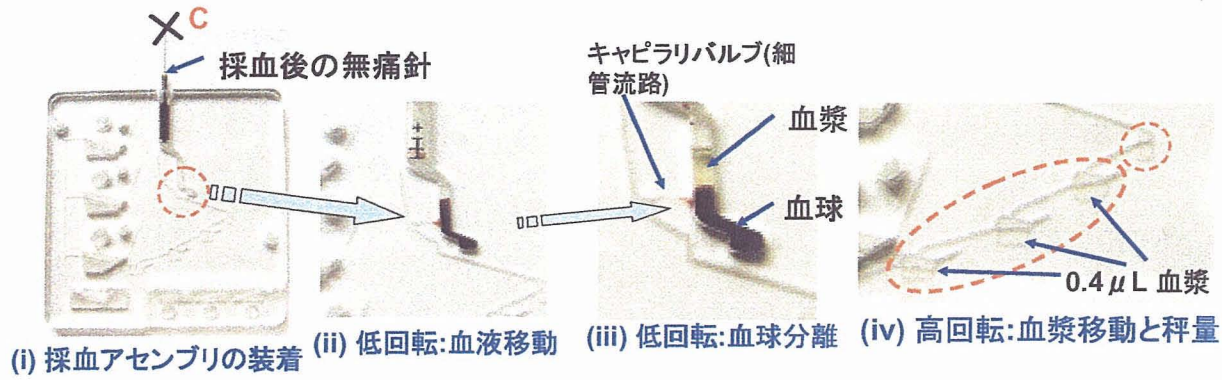

図 7　血球･血漿分離、血漿秤量遂行の様子

させて、血球･血漿分離を進行させた後（同図(iii)）、チップの回転数を 3000rpm として印加遠心力を増加させ、分離した血漿成分をキャピラリバルブを通過させ、下流の血漿秤量層を満たし、血漿を秤量する。（同図(iv)）以上の様に、血球･血漿分離、血漿秤量が遂行できていることを確認した。

C.2 試薬等の移送の様子

チップ回転時に生起する遠心力により、試薬や血液の移動の様子を図 8 に示す。まず同図(a)に示すように試液 A と B を同時にチップに注入する。観察を容易にするためにここでは色素溶液を用いている。また同時に血液を模し、赤色色素溶液も採血モジュール導入口から注入している。以前のチップでは、この時点では試液 A のみ注入しており、B は後から注入していたが改良型の本チップではこのように同時に注入するようにした。次に同図(b)に示すように X の回転中心にしてチップを回転させ、試液 A ならびに B をそれぞれ秤量する。また同時に血液も血球・血漿分離と血漿の秤量を行っている。次に同図(c)に示すようにチップを 90 度回転させ、図中の X を中心軸としてチップを回転させる。すると秤量した血漿と試液

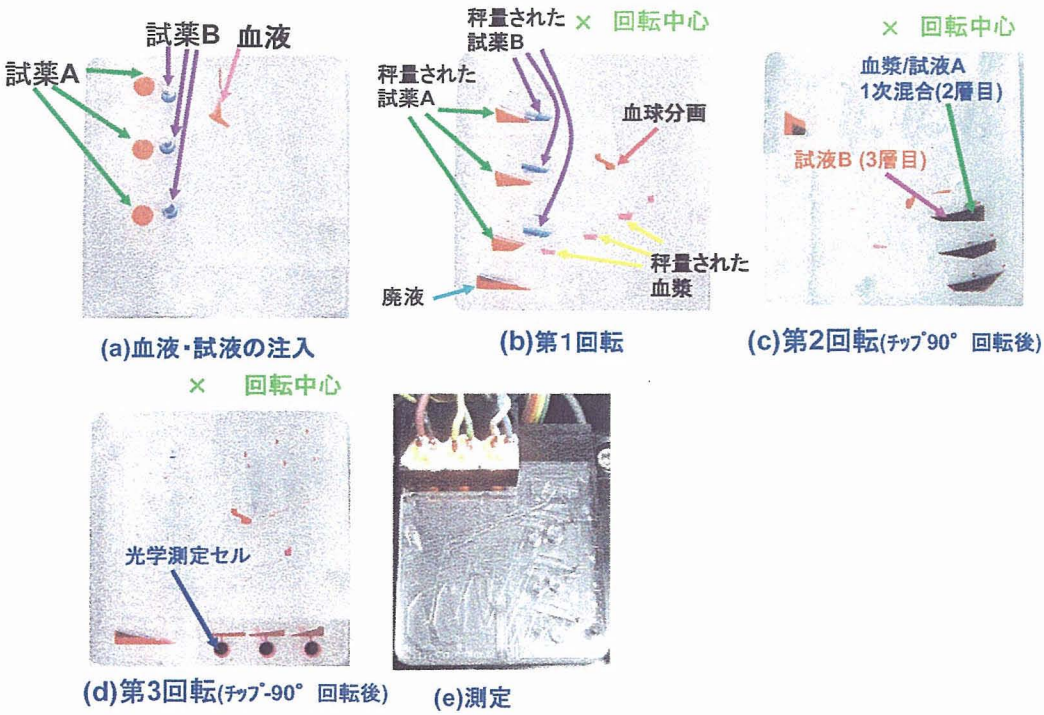

図 8　チップ内での試液等の移送の様子

Aがそれぞれの一次混合槽で混合される。本混合槽と完全に重畳しているために観察しにくいが、下層には試液Bが移送されてきている。そして再度チップを-90度回転させて、同図(d)のXを中心軸として回転させると、(血漿＋試液A)と試液Bが混合流路を経て、均質に混合されて光学測定セルへと移送される。混合流路については昨年度報告したような方式を踏襲している。そしてこのときの特定波長の光の吸収強度を同図(e)のように吸光度測定により求め、これを濃度に換算する。以上のようにして試液や血液、血漿の移送、秤量、混合などを遂行できることを確認した。

C.3 自動計測装置

図8に示したような、チップの自転回転、公転回転、温調、吸光度測定などを自動的に行う装置を作製して評価を行っている。(図9) 本装置のチップをマウントするステージ部など若干の改良箇所があるが、概ね良好に動作している。長時間の耐久試験などは今後の課題である。

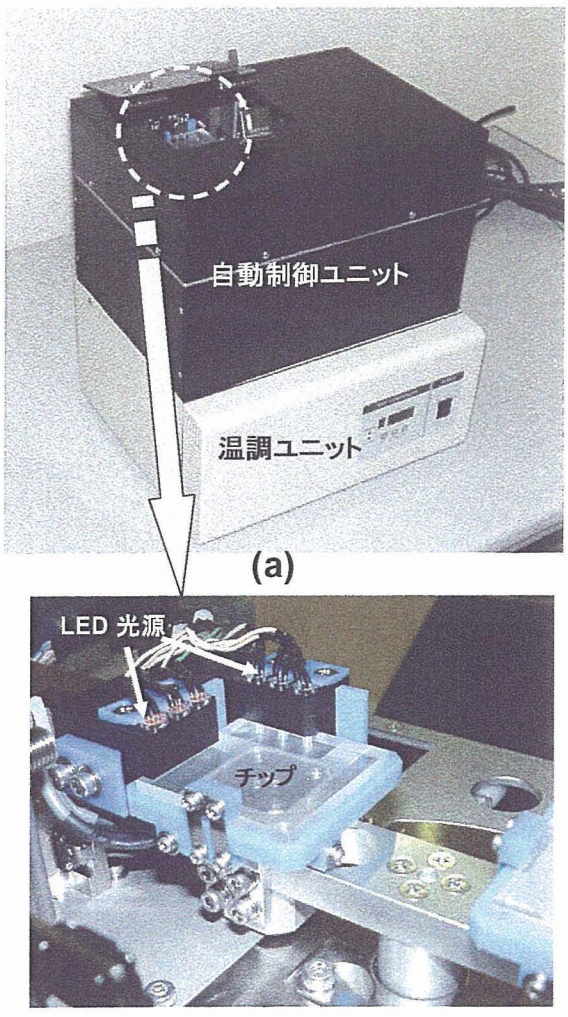

図9　自動計測装置

C.4 3項目測定例

中性脂肪、総コレステロール、HDLコレステロールの血中脂質3項目を測定した例を示す。図10のように無痛針採血モジュールを用い、血液を約6μL採取し、この分析をチップを用いて行った。この被験者の平成18年6月8日の定期健康診断時の測定値は表1に示す通りで、特に中性脂肪は、許容値が50～149mg/dLに対して281mg/dLと許容値を逸脱し高値となっている点が特徴である。実際、この方は高脂血症と医師に診断されている。本チップでの検査は平成18年10月28日に行い、結果は図11に示すように総

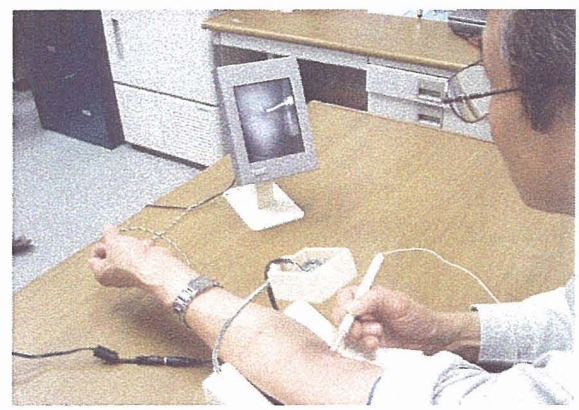

図10　採血の様子

表1　定期健康診断時の測定値

総ｺﾚｽﾃﾛｰﾙ	150- 219	233	B
中性脂肪	50- 149	281	B
ＨＤＬｺﾚｽﾃﾛｰﾙ	40- 80	67	A

図11　採血の様子

コレステロール 236mg/dL、中性脂肪 303mg/dL、HDL コレステロール 55mg/dL であり、やはり定期健康診断のときと同様に中性脂肪が特に高値であることが特徴となっており、符合している。このようなチップの評価は、同一検体を従来の大型分析装置とチップを用い測定し、その結果を比較してチップの評価を行う予定である。

D. 健康危険情報

特に無し。

E. 研究発表

1. 論文発表

R. Ogawa, H. Ogawa, A. Oki, S. Hashioka, Y. Horiike, "Fabrication of nano-pillar chips by a plasma etching technique for fast DNA separation" Thin Solid Films **515** (2007) pp.5167–5171.

2. 学会発表

小川洋輝、長井政雄、堀池靖浩"微量血液分析ヘルスケアチップの開発" 第 45 回日本生体医工学会大会 2006 年 5 月

3. 解説

堀池靖浩、甲田裕子、小川洋輝、長井政雄、"無痛針による微量採血分析から在宅で健康診断できるヘルスケアチップの開発"、臨床検査、(2006) **50**、pp.1557-1565.

F. 知的財産権の出願・登録状況

(予定を含む。)

1. 特許出願

なし。

2. 実用新案登録

なし。

3. その他

なし。

III. 研究成果の刊行に関する一覧表
書籍

著者氏名	論文タイトル名	書籍全体の編集者名	書　籍　名	出版社名	出版地	出版年	ページ
堀池靖浩 宮原裕二	バイオチップとバイオセンサー	高分子学会	高分子先端材料 One Point バイオチップとバイオセンサ	共立出版	東京都	2006年	1～65 139～173

雑誌

発表者氏名	論文タイトル名	発表誌名	巻号	ページ	出版年
R.Ogawa, H.Ogawa, A.Oki, S.Hashioka, Y.Horiike	Fabrication of nano-pillar chips by a plasma etching technique for fast DNA separation	Science.Direct	515	5167-5171	2006
Noritake.Kaji Ryo Ogawa Akio Oki Yasuhiro.Horiike Manabu Tokeshi Yoshinobu Baba	Study of water properties in nanospace	Anal Bioanal Chem	386	759~764	2006
堀池靖浩 甲田裕子 小川洋輝 長井政雄	無痛針による微量採血分析から在宅で健康診断できるヘルスケアチップの開発	ナノテクノロジーとバイオセンサ　各論Ⅲ．マイクロチップ分析関連	第50巻12号増刊号	1557-1565	2006
Shinji Fukumoto Taiju Matsuo Daisuke Kuroda Harushige Tsubakino	Midro-Resistance Spot Welding of Nickel Free Austenitic Stainless Steel	Materials Science Forum	539-543	4081-4086	2007
黒田大介	Niフリーステンレス鋼	金属	77	148-154	2007

学会発表

種別	著者	発表題目	会議名	開催期間	開催地	発表誌名	ページ
口頭発表	黒田大介 檜原高明 黒田秀治 藤原昌樹 堀池靖浩	窒素により高剛性化した無痛針の機械的特性	日本高専学会第１２回年会講演会	2006/08/19 - 2006/08/20	神戸	講演論文集	55-56
口頭発表	小川涼 加地範匡 若尾創 橋岡真義 馬場嘉信 堀池靖浩	矩形配列ナノピラーによる DNA 慣性半径に基づく DNA サイズ分離効果	2006年秋季 第67回応用物理学会学術講演会	2006/08/28 - 2006/09/01	滋賀	講演予稿集	31
口頭発表	橋岡真義 小川涼 堀池靖浩	マイクロピラーおよびハイドロゲルバルブを利用した DNA 前処理チップの作製	2006年秋季 第67回応用物理学会学術講演会	2006/08/28 - 2006/09/01	滋賀	講演予稿集	31
口頭発表	Ryo Ogawa Noritada Kaji Shingi Hashioka Yoshinobu Baba Yasuhiro Horiike	DNA Size Separation Employing Quartz Nano-Pillars with Different Allocations	The 2006 Onternational Conference on Solid State Devices and Materials	2006	Yokohama	Extended Abstracts	870-871
口頭発表	Shingi Hashioka Ryo Ogawa Hiroki Ogawa Yasuhiro Horiike	Integrated DNA Purification and Detection Device for Diagnosis of Infection Diseases	The 2006 Onternational Conference on Solid State Devices and Materials	2006	Yokohama	Extended Abstracts	872-873
口頭発表	堀池靖浩 甲田裕子 張嘉顯 小川涼 橋岡真義 長井政雄 小川洋輝	COLORIMETRIC MEASUREMENT CLINICAL CHIP FOR HOME MEDICAL DIAGNOSIS	μTAS2006	2006/11/05-2006/11/09	東京	Micro Total Analysis Systems 2006	Page 1558～1560/

口頭発表	小川涼 加地範匡 若尾創 橋岡真義 馬場嘉信 堀池靖浩	ナノ構造体を用いた DNA サイズ分離機序の解明	第 28 回日本バイオマテリアル学会大会	2006/11/27 - 2006/11/28	東京	予稿集	114
口頭発表	橋岡真義 小川涼 堀池靖浩	DNA ワンチップ診断のための前処理デバイスの作製	第 28 回日本バイオマテリアル学会大会	2006/11/27 - 2006/11/28	東京	予稿集	304
口頭発表	堀池靖浩 甲田裕子 張嘉顯 小川涼 橋岡真義 長井政雄 小川洋輝	在宅診断用比色測定検診チップ	NANOBIO-TOKYO 2006	2006/12/04-2006/12/07	東京	Extended Abstract of NANOBIO — TOKYO 2006	Page 379～380/
口頭発表	堀池靖浩	ドライ比色法による微量血液分析在宅診断チップ	第１回ナノバイオテクノロジー連携群 成果報告会	2006/12/21	東京		
口頭発表	堀池靖浩 甲田裕子 張嘉顯 長井政雄 小川洋輝	ドライ比色法による微量血液分析在宅診断チップ	萌芽的先端医療技術推進研究事業に係る研究成果発表会	2007/02/13	東京	要旨集	37-39
口頭発表	Chang Chia-Hsein Hiroki Ogawa Hashioka Shingi Yasuhiro Horiike	Droplet device aiming to be used for multiple immunoassay detection	第 54 回応用物理学関係連合講演会	2007/3/27-2007/3/30	東京	講演予稿集	1371
口頭発表	橋岡真義 益一哉 堀池靖浩	前処理デバイスを搭載したナノギャップ DNA 診断チップの作製	第 54 回応用物理学関係連合講演会	2007/3/27-2007/3/30	東京	講演予稿集	1371

Available online at www.sciencedirect.com
ScienceDirect
Thin Solid Films 515 (2007) 5167–5171
www.elsevier.com/locate/tsf

Fabrication of nano-pillar chips by a plasma etching technique for fast DNA separation

R. Ogawa *, H. Ogawa, A. Oki, S. Hashioka, Y. Horiike

National Institute for Materials Science (NIMS), Tsukuba, Ibaraki, 305-0044, Japan

Available online 27 November 2006

Abstract

The fabrication of quartz nano-pillars was investigated using dry etching with a Ni mask. The mask diameter increased during etching due to re-sputtering of the Pt/Cr seed layer. However, once the seed layer had been eroded the enlarged mask diameter did not increase any further. Hence, the use of the mask enabled the fabrication of nano-pillars with a high aspect ratio. In situ FTIR–ATR observation of HF quartz plate pressure bonding developed a new bonding technique involving the use of H_2SiF_6. The nano-pillar chips allowed then to size-separate DNA of 10 kbp and 38 kbp within 20 s.

Keywords: Nano-pillars; Quartz bonding; DNA electrophoresis; DNA size separation

1. Introduction

After 100% of the human genome project was deciphered in 2003, studies in genomics are now advancing towards tailor-made medical treatments according to individual genome information. This goal requires a new DNA separation technique that is between 10^8 and 10^9 times faster than current separation methods such as gel based capillary electrophoresis. In addition, it will be necessary to separate DNA fragments that may be several tens of kilobases in length. Existing techniques such as pulsed-field gel electrophoresis [1–3] suffer from decreased separation resolution as the length of the DNA fragment increases. To overcome these issues, microfluidic devices with nano-structures are being studied as an alternative to gel electrophoresis. For example, Craighead et al. reported a technique for the separation of circular (M13) and linear lambda DNA [4] employing nano-pillars, and the device showed the function as a molecular sieve. Also, the size-separation of DNA [5–7] was reported by Craighead et al., based on entropy trapping employing microfabricated nano-structures. Those devices for DNA separation were fabricated using lithographic techniques. Arrays of self-assembled magnetic bead columns were also investigated and used to separate DNA fragments of tens of kilo base pairs (kbp) [8,9].

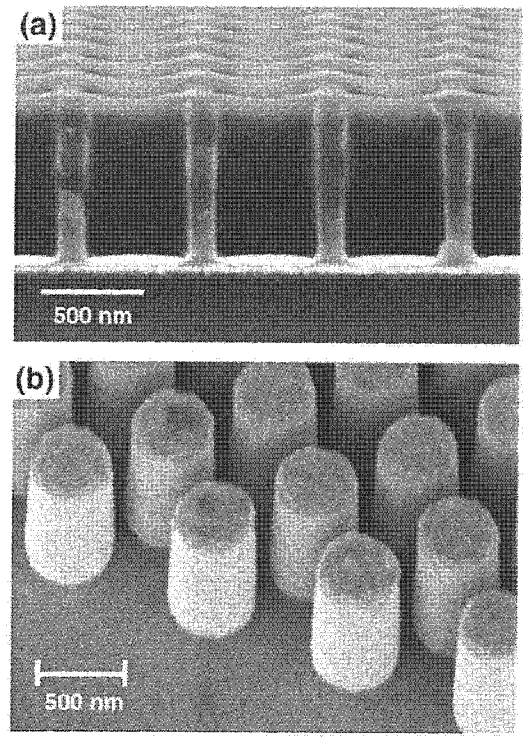

Fig. 1. (a) Cross-sectional SEM picture of the resist hole pattern and (b) of the Ni posts after removal of the resist, viewed at an angle of about 45°.

* Corresponding author.
E-mail address: Ogawa.ryo@nims.go.jp (R. Ogawa).

0040-6090/$ - see front matter © 2006 Elsevier B.V. All rights reserved.
doi:10.1016/j.tsf.2006.10.072

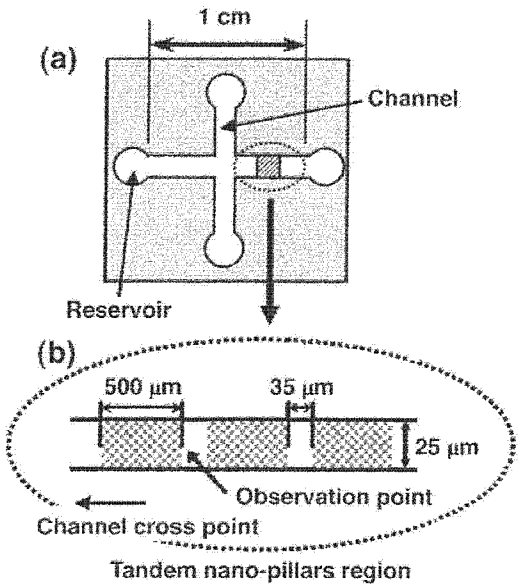

Fig. 2. (a) Schematic of the channel layout and (b) enlarged view of the separation channel, showing regions with and without nano-pillars.

Previously, we demonstrated the electrophoretic separation of DNA in a microchannel containing an array of nano-pillars. With this technique, we were able to reduce the time required for the separation of T4-DNA (166 kbp) and λDNA (48.5 kbp) from half a day for conventional gel electrophoresis to just 25 s [10]. Furthermore, by employing a channel with regions with and without pillars permitted the multi-stage separation of DNA fragments from 100 bp to 1 kbp. The microfluidic devices were fabricated using quartz substrates. The use of quartz prevented dielectric breakdown when applying the high electric fields required for the electrophoretic separation of DNA and also permitted the observation of fluorescently labeled DNA molecules excited using ultraviolet light.

This paper describes the technologies involved in the fabrication of nano-pillars on a quartz plate, and a new bonding technique for quartz plates based on elucidation of the mechanism responsible for 1% HF bonding [11] using FTIR–ATR (Fourier transform Infrared–Attenuated Total Reflection). The separation of DNA using these nano-pillar chips is also reported.

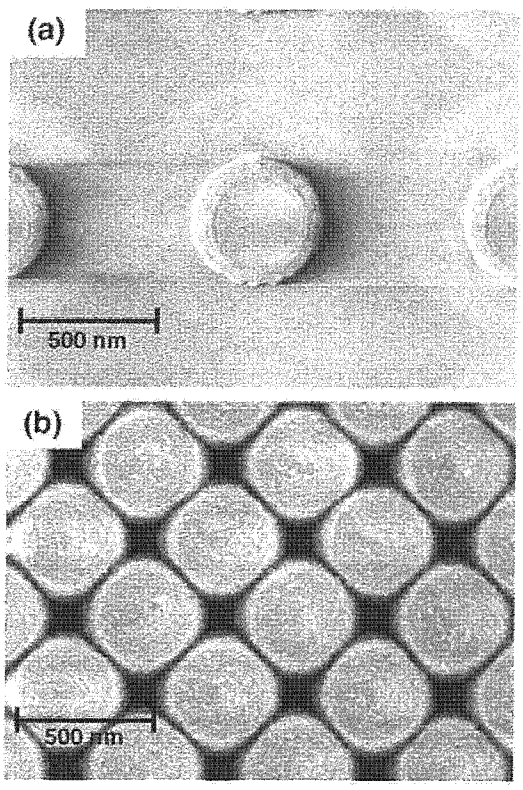

Fig. 3. SEM pictures of quartz nano-pillar patterns after one minute of etching, where the center-to-center distance of the Ni mask was (a) 1 μm and (b) 600 nm. The initial diameter of the Ni masks was 450 nm.

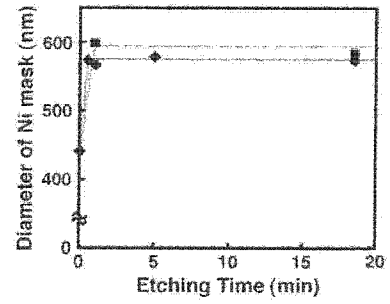

Fig. 4. Ni mask diameter changing with time for a center-to-center distance of 600 nm (◆) and those of 1 μm (■).

2. Experimental

2.1. Nano-pillar fabrication

A 0.5 mm thick quartz wafer was sputter-coated with a Pt/Cr seed layer. The layer thickness ranged from 50 to 70 nm due to

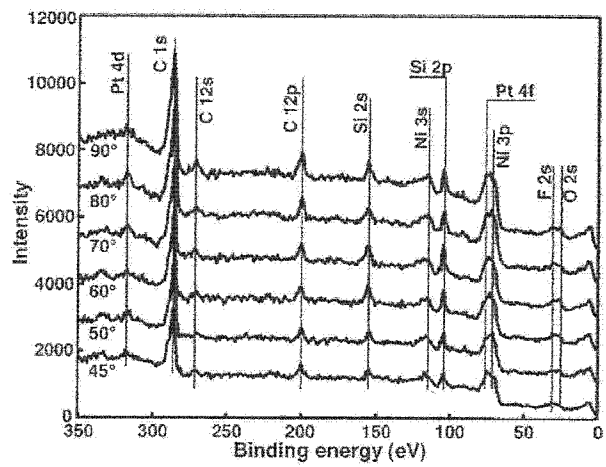

Fig. 5. Angular dependent XPS spectra of a quartz surface with Ni masks after etching for 1 min.

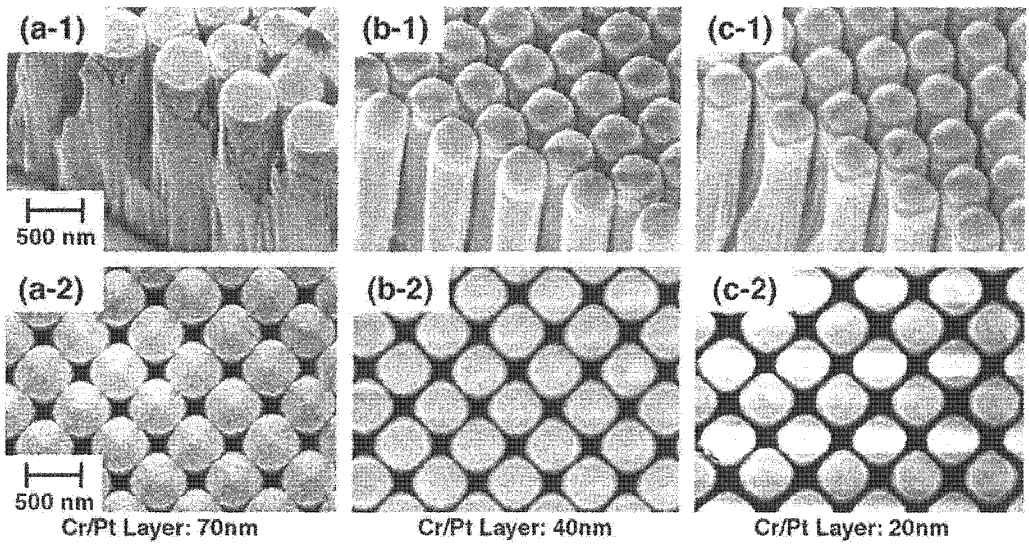

Fig. 6. SEM pictures of nano-pillars formed by the etching of substrates with different Pt/Cr seed layer thicknesses: (a) for 70 nm, (b) for 50 nm and (c) for 20 nm. The top row of figures is viewed at an angle of about 45° while the bottom row of figures is viewed from above.

the instability of our sputter–deposition system. This wafer was then spin coated with an electron beam (EB) resist (ZEP-520A, Nippon Zeon). This resist was patterned with an array of 500 nm diameter holes using EB lithography (ELS-7500, Elionix). Ni was then electroplated into the array of holes left in the resist. The remaining resist was removed, leaving an array of 450 nm diameter Ni pillars (see Fig. 1). The substrate was then etched by employing Neutral Loop Discharge (NLD) [12] with CF_4. Ni and quartz etch rates were 21.5 nm/min and 238 nm/min, respectively, thus leading to a selectivity of 12 for quartz relative to Ni. After removal of the Ni mask by wet etching, the substrate was pressure bonded to a 130 μm thick quartz top plate that had been dipped into H_2SiF_6. A pressure of 1 MPa was applied for 12 h at 65 °C.

2.2. DNA electrophoretic separation

A schematic of a fabricated nano-pillar chip with two intersecting channels is shown in Fig. 2(a). Each channel was 1 cm in length, 25 μm in width, and 4 μm in depth. 500 μm long regions of nano-pillars were arranged along the separation channel with a spacing of 35 μm between each region, as shown in Fig. 2(a) and (b). The electrophoretic behavior of individual DNA molecules (T4 DNA, 166 kbp) was observed using a fluorescence microscope with a water immersion lens (see Fig. 10). For these observational experiments, the applied electric field was 25 V/cm. λDNA was digested into 10 kbp and 38 kbp fragments by *Apa*I. The electrophoretic separation of DNA was investigated by electrically injecting a plug of a sample containing *Apa*I digested fragments into the separation channel of a nano-pillar chip. The DNA fragments were 10 kbp and 38 kbp in length, and the electric field in the separation channel was 100 V/cm. The fluorescent intensity of DNA labeled with YOYO-1 was observed at a point 500 μm downstream from the last nano-pillar region.

3. Results and discussion

3.1. Increase in diameter of Ni pillars after etching

Fig. 3(a) and (b) show overhead views of quartz pillar patterns after etching for 1 min using Ni masks with an original diameter of 450 nm, where center-to-center distances of the Ni masks for (a) and (b) were 1 μm and 600 nm, respectively. The diameter of the quartz pillars in (a) increased to 600 nm. The pillars in (b) formed a pseudo-square shape with a side-to-side width of 520 nm and a diagonal width of 690 nm. In this paper, the inter-pillar gap is defined as the nearest distance between pillars. For example, a center-to-center distance of 600 nm with 500 nm diameter pillars corresponds to a 100 nm gap. Thus in case (b), the gap for the side-to-side direction was about 30 nm.

In order to investigate the origin of the increase in diameter of the quartz pillars after etching, the time-dependent variation of Ni mask diameter was measured for both (a) and (b) as shown in Fig. 4. For case (a), within 1 min, the diameter of the Ni

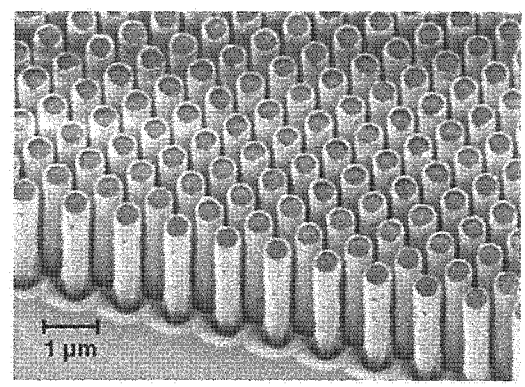

Fig. 7. SEM picture of nano-pillars with a diameter of 500 nm, an inter-pillar gap of 100 nm, and an aspect ratio of 8.

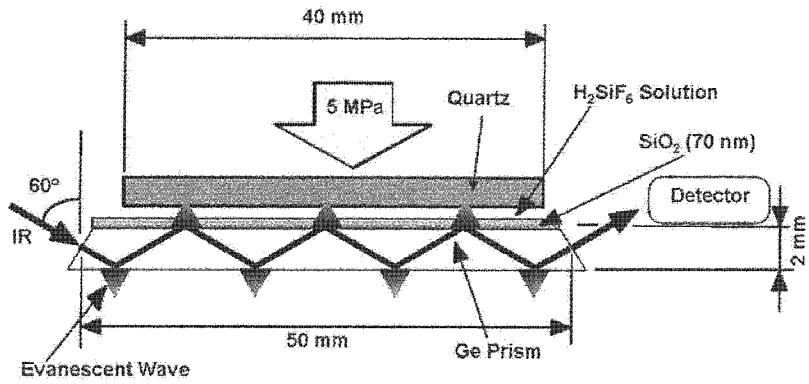

Fig. 8. Schematic cross section of the specimen used for *in situ* FTIR–ATR observation of the pressure bonding process.

pillars increased to 600 nm, and in case (b), within 1 min, the side-to-side width increased to 570 nm. Subsequently they did not increase any further. It is revealed that the increase of diameter in Ni pillar led the diameter of quartz pillar to increase. The entire surface including pillars was analyzed using XPS (X-ray photoelectron spectroscopy, Quantera, PHI). Fig. 5 shows the result of an angular-dependent XPS measurement, where specimen angles were changed from 45° to 90°. Spectra were acquired from substrates that had been etched for 5 min. Peaks corresponding to carbon/fluorine and Ni originating from the etching gas and the mask were clearly detected. Although no significant differences between angular-dependent spectra were observed, the peak at 315 eV was evaluated to result from the 4d orbital of Pt. Hence it is likely that the surface of the Ni mask is covered with the sputtered Pt–Cr seed layer. Peaks from Cr could not be detected because the strong peaks of Cr overlapped with the peaks of oxygen. These results demonstrate that the sputtered Pt–Cr film re-attaches to the sidewalls of the Ni mask in the initial stage of quartz etching. Once the Pt/Cr seed layer has been eroded, there is no more material available for re-attachment and the mask diameters do not change any more (Fig. 4). Therefore the thickness of the Pt/Cr seed layer was altered to see what effect that would have on the morphology of the etched pillars as shown in Fig. 6. When the thickness of the Pt/Cr seed layer was 70 nm, adjacent Ni masks almost overlapped with each other after etching due to re-attachment.

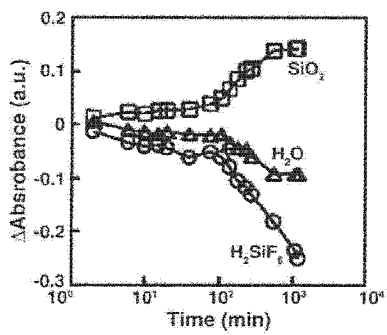

Fig. 9. FTIR–ATR absorbance changes of: SiO_2 (1070 cm^{-1}, □), H_2O (1650 cm^{-1}, Δ) and H_2SiF_6 (739 cm^{-1}, ○).

However, the gaps between Ni masks after etching did not disappear for Pt/Cr seed layer thicknesses of 50 nm and 20 nm. Hence, by using a thinner seed layer, a regular array of high aspect ratio quartz nano-pillars could be fabricated, as shown in Fig. 7 for 500 nm pillars with a 100 nm gap and an aspect ratio of 8.

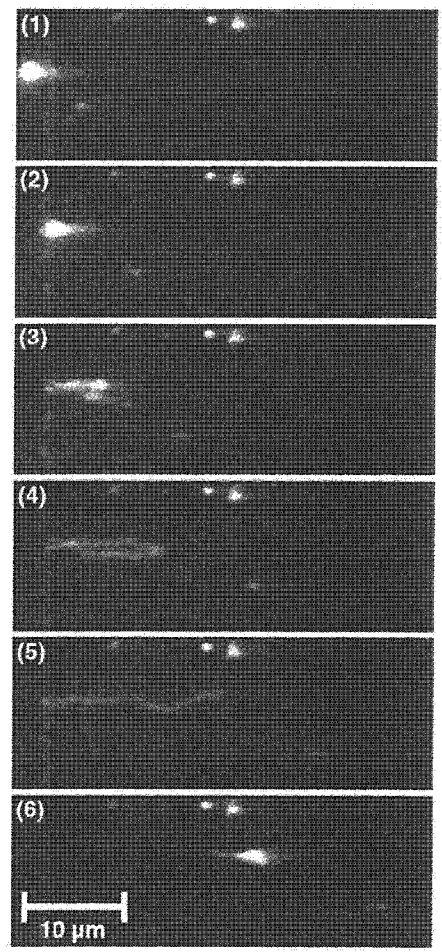

Fig. 10. A series of photographs of the single molecule electrophoretic behavior of T4 DNA (166 kbp) in the nano-pillar chip.

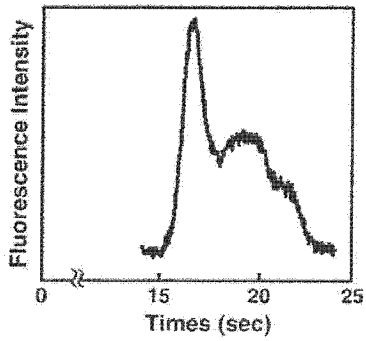

Fig. 11. Electropherogram of the separation of 10 kbp and 38 kbp DNA in the nano-pillar chip.

3.2. Quartz bonding using H_2SiF_6

Fracturing of the quartz plates was often encountered when employing 1% HF dipping and subsequent pressure bonding at 1.3 MPa [11] to bond the 130 μm thick quartz cover plate onto the patterned substrate. In order to improve this bonding technique we investigated the mechanism responsible for bonding. We prepared a FTIR–ATR (Fourier Transform Infrared–Attenuated Total Reflection) system as shown in Fig. 8, in which a SiO_2 layer of 70 nm thickness was sputter-deposited onto the surface of a Ge prism. A quartz plate was dipped in 10% HF and then pressed onto the SiO_2/Ge surface at 5 MPa. Time-dependent changes of absorbance due to the formation of products were investigated. The results revealed clearly that the interface of the quartz plates was first etched by the HF solution, thereby producing H_2O and H_2SiF_6 as products. Subsequently, SiO_2 was formed at the interface as a result of H_2O and SiF_4 elimination. During measurements, we noted the growth and then diminution of the H_2SiF_6 adsorption peak. It occurred to us that since the H_2SiF_6 was responsible for SiO_2 formation at the interface, then H_2SiF_6 could be utilized directly as a bonding agent. Fig. 9 shows time-dependent changes of the SiO_2, H_2O and H_2SiF_6 absorption peaks. Both H_2O and H_2SiF_6 peaks decreased as the amount of SiO2 increased. Based on these results, a quartz plate was dipped in H_2SiF_6 solution and then placed in contact with another quartz plate. A satisfactory bond was achieved when these plates were subjected to a pressure of 1 MPa at 65 °C for 12 h. These conditions were milder than those required for the 1% HF dipping technique.

3.3. DNA size separation

The single molecule behavior of T4 DNA (166 kbp) in the nano-pillar regions was observed and this is shown in Fig. 10. DNA underwent repeated cycles of shrinking, stretching, and hooking. The DNA fragments did not follow a straight path and often changed direction. This behavior suggests that the nano-pillars play a role that is analogous to the sieving effect that occurs when using a polymer matrix in gel electrophoresis. The electrophoretic speed of the DNA fragments in the pillar-covered regions was 31.4 μm/s. The separation of 10 kbp and 38 kbp DNA fragments obtained from *ApaI* digested λDNA was investigated using a nano-pillar chip with a pillar gap of 100 nm. An electropherogram of this separation is shown in Fig. 11. Two peaks can be observed, indicating the successful separation of 10 and 38 kbp DNA within 20 s.

4. Conclusions

Nano-pillars were fabricated by dry etching using a Ni mask. The mask diameter increased from 450 nm to 570 nm during the etching process. This was caused by reattachment due to sputtering of the Pr/Cr seed layer on the quartz plate substrate. The growth of the Ni mask stopped once the seed layer had been eroded by the etching process and thus nano-pillars with high aspect ratios could be fabricated. An investigation of the quartz HF dip-bonding mechanism with in situ FTIR–ATR led to the development of a more effective bonding method involving the use of H_2SiF_6. The nano-pillar chip fabricated using these technologies allowed us to separate 10 kbp and 38 kbp DNA fragments within 20 s.

Acknowledgements

The authors would like to express our great thanks to Dr. Alexander Iles of the National Institute for Materials Science who corrected carefully English.

This research was partially supported by the Ministry of Education, Science, Sports and Culture, Grant-in-Aid for Young Scientists (B), 17750078 6822, 2005 and the Advance Nano-Bio Device Project (P03011) supported by NEDO (New Energy and Industrial Technology Development Organization).

XPS analysis was supported by the Material Analysis Station of the National Institute for Materials Science.

References

[1] M. Lalande, J. Noolandi, C. Turmel, J. Rousseau, G.W. Slater, Proc. Natl. Acad. Sci. U. S. A. 84 (1987) 8011.
[2] G.W. Slater, J. Noolandi, J. Rousseau, C. Turmel, M. Lalande, Biophys. J. 53 (1988) A475.
[3] C. Turmel, E. Brassard, G.W. Slater, J. Noolandi, Nucleic Acids Res. 18 (1990) 569.
[4] S.W. Turner, A.M. Perez, A. Lopez, H.G. Craighead, J. Vac. Sci. Technol., B 16 (1998) 3835.
[5] J. Han, S.W. Turner, H.G. Craighead, Phys. Rev. Lett. 83 (1999) 1688.
[6] J. Han, H.G. Craighead, Science 288 (2000) 1026.
[7] J. Han, H.G. Craighead, Anal. Chem. 74 (2002) 394.
[8] P.S. Doyle, J. Bibette, A. Bancaud, J.-L. Viovy, Science 295 (2002) 2237.
[9] N. Minc, C. Fütterer, K. Dorfman, A. Bancaud, C. Gosse, C. Goubault, J.-L. Viovy, Anal. Chem. 76 (2004) 3770.
[10] N. Kaji, Y. Tezuka, Y. Takamura, M. Ueda, T. Nishimoto, H. Nakanishi, Y. Horiike, Y. Baba, Anal. Chem. 76 (2004) 15.
[11] H. Nakanishi, T. Nishimoto, M. Kanai, T. Saitoh, R. Nakamura, T. Yoshida, S. Shoji, Sens. Actuators 83 (2000) 136.
[12] Y. Chinzei, M. Ogata, H. Shindo, T. Ichiki, Y. Horiike, J. Vac. Sci. Technol., A 16 (1998) 1519.

Anal Bioanal Chem (2006) 386: 759–764
DOI 10.1007/s00216-006-0469-3

ORIGINAL PAPER

Noritada Kaji · Ryo Ogawa · Akio Oki · Yasuhiro Horiike · Manabu Tokeshi · Yoshinobu Baba

Study of water properties in nanospace

Received: 27 January 2006 / Revised: 3 April 2006 / Accepted: 5 April 2006 / Published online: 25 May 2006

Abstract Here we report an anomalous behavior of water, especially its viscosity and hydrodynamic flow, in a nanometer-confined space. As a typical model of a nanometer-confined space, the nanopillar chip, which was developed for DNA size-based separation was used, and single-particle tracking (SPT) technique was applied to investigate water viscosity and hydrodynamic flow in the nanopillar chip. The diffusion coefficients of nanospheres were almost one-third of the theoretical value derived from the Stokes-Einstein equation. This result gave indirect proof that water viscosity in a nanometer-confined space is higher than in a bulk solution. In order to improve resolution and throughput of the nanopillar chip for DNA separation, these potential factors affecting performance should be seriously considered.

Keywords Diffusion coefficient · Nanospace · Nanoparticles · Single-particle tracking · Nanopillar chip

Abbreviations SPT: Single-particle tracking · ICP: Inductively coupled plasma

N. Kaji (✉) · M. Tokeshi · Y. Baba
Department of Applied Chemistry,
Graduate School of Engineering,
Nagoya University,
Furo-cho, Chikusa-ku,
Nagoya 464-8603, Japan
e-mail: kaji@apchem.nagoya-u.ac.jp
Tel.: +81-52-7894611
Fax: +81-52-7894666

R. Ogawa · A. Oki · Y. Horiike
Nanomaterials Laboratories,
National Institute for Materials Science,
1-1, Namiki,
Tsukuba 305-0044, Japan

Y. Baba
Health Technology Research Center, National Institute of Advanced Industrial Science and Technology,
Hayashi-cho 2217-14,
Takamatsu 761-0395, Japan

Noritada Kaji
is Assistant Professor in the Department of Applied Chemistry at Nagoya University. His current research interests are mainly divided into three parts: nano-biodevices for DNA analysis, single molecule biophysics, and biological process on μTAS.

Introduction

Nanotechnologies, especially top-down approaches to construct nanometer-sized structures, have made it possible to fabricate sub-micrometer-sized channels and structures on silicon and quartz substrate. Now the sub-micrometer channels and structures are available for not only mechanical and electrical engineers but also analytical chemists. Nanospace, more precisely sub-micrometer space, is a quite interesting space especially for biophysicists because most biomolecules are nanometer-sized and are expected to show novel physical effects in nanospace [1–5]. What is more, a variety of studies of the physicochemical properties of liquids confined in nanospace have been performed, and it is indicated that liquid properties change in nanospace as compared with bulk. Tas et al. determined the negative pressure in nanochannels from the liquid meniscus [6] and Liu et al. gave an insight into unique properties in a confined liquid through the measurement of ion transport [7] and proton conductivity [8]. Tsukahara et al. proposed water structures in nanochannels based on NMR study [9, 10] and Hibara et al. investigated liquid viscosity and conductance in nanochannels by time-resolved fluorescence measurements [11]. Water confined in carbon nanotubes, which give an ultimately confined nanospace, has also been extensively studied experimentally [12, 13] and computationally [14]. These changes in liquid proper-

ties are of great interest in basic science. In order to develop our DNA separation method using the nanopillar chips, several investigations into hydrodynamic properties in nanospace are necessary to improve resolution and throughput. Since the surface area of the nanopillar chip is much larger than simple channel structures, it is readily understood that such a large, charged surface area raises complex electroosmotic flow and adsorption probabilities and may affect the analysis [15].

To investigate the liquid properties, we applied the single-particle tracking (SPT) technique to measure water viscosity in nanospace. A major advantage of the SPT technique is the ability to classify modes of Brownian motion of individual particles. Using this technique, it has been observed that individual membrane proteins or lipids in the plasma membrane of cells show a variety of types of motion, such as normal diffusion, directed diffusion, and restricted diffusion [16–18]. This variety of motions has been attributed to the presence of a random energetic trap array with different binding energies. In an ensemble of long-time averages, the mean-square displacement as a function of time revealed characteristics of the motion. Additionally, the slope of a mean-square displacement vs. time plot would give the diffusion coefficient that reflects the ambient viscosity. Taking these advantages into consideration, we applied the SPT technique to measure water viscosity and verify the presence of a hydrodynamic flow in nanospace.

Materials and methods

Device fabrication and design

The fabrication process of the nanopillar chip used here was the same described in our previous work [19] except the SiO_2 dry etching process. In this fabrication process, the quartz plate was etched by Cl_2 inductively coupled plasma (ICP). To investigate liquid properties in nanospace using SPT technique, the use of a quasi two-dimensional plane that allows observation of two-dimensional single-particle motion, would be preferable. From this standpoint, a shallow channel is preferable to let the molecules move in a quasi two-dimension plane. In addition, to acquire the precise trajectories without any special optical systems, a shallow channel provides optimum observation space since the focal depth of the high-power objective lens is only a few hundred nanometers, e.g., 150 nm for 100x/1.3 NA

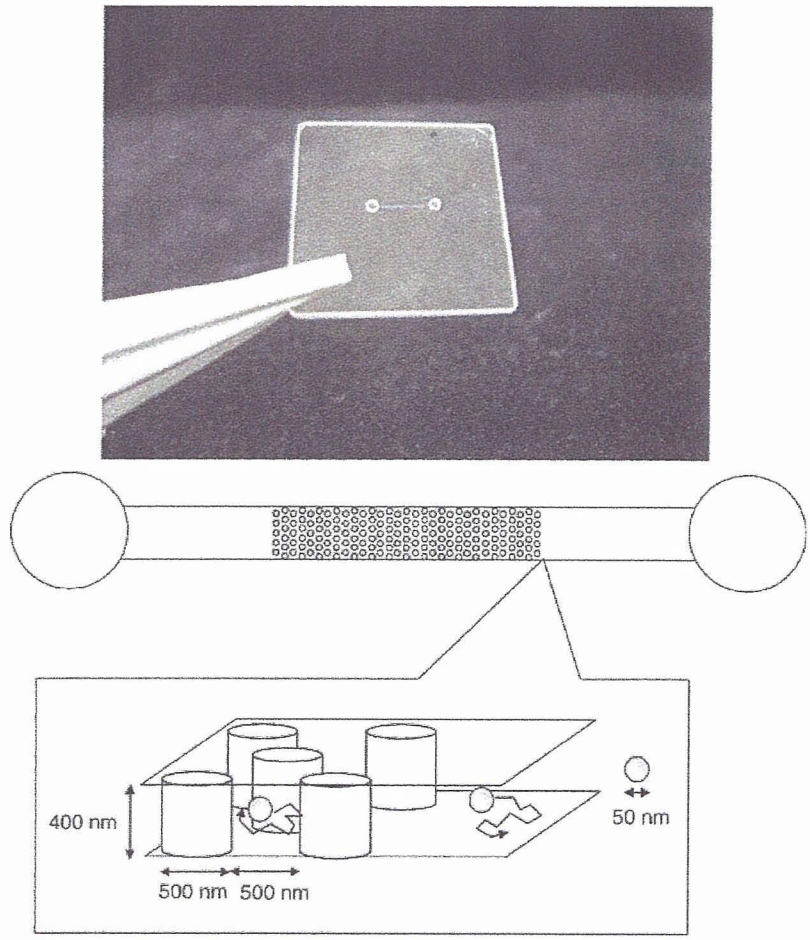

Fig. 1 Schematic representation of the nanopillar chip used for a single-particle tracking (SPT) measurement. The channel width and depth were 50 μm and 400 nm, respectively. Nanopillars were placed in the middle section of the channel, and their diameter, spacing and height were 500, 500, and 400 nm, respectively

objective lens. In order to observe the trajectories in this shallow channel through a 100x objective lens, a 0.17-mm-thick cover slip is required for the highest image resolution. Considering these points, a 400-nm-deep channel equipped with nanopillars in its middle section was fabricated on quartz substrates as shown in Fig. 1. The nanopillar diameter, spacing, and height used here were 500, 500, and 400 nm, respectively.

Single-particle tracking

Fluorescent polystyrene nanospheres with carboxylate groups on their surfaces (3.64×10^{14} particles/ml, 50 nm in diameter, Fluoresbrite YG Carboxylate Microspheres, Polysciences, Warrington, PA) were used as objective particles for measuring trajectory. The size and the ζ potential of nanospheres were confirmed by dynamic light scattering (DLS) and electrophoretic light scattering (ELS), respectively, using a dynamic light-scattering spectrophotometer (NICOMP 380/ZLS, Particle Sizing Systems, Santa Barbara, CA). Before the size measurement, the nanospheres were diluted 100-fold in deionized water and sonicated for 15 min to break up aggregates. The nanospheres had a diameter of 50.0±5.5 nm and a ζ potential of −44 mV in deionized water.

The chip was rinsed with 1 M HCl, 1 M NaOH and deionized water before use to remove any contaminants on the channel and the pillar surfaces. Owing to the treatment with sodium hydroxide, the minus-charged nanobeads could continue Brownian motion against adsorption on the surfaces. The washing procedure for nanopillar chips is one of the critical problems. In our first attempt, we tried to wash the nanopillar chip with a pressure-driven flow. But due to the infinitesimally small quantity of the solution in the nanopillar chip (~pl) and frangible nanopillars, this washing method seemed to be inappropriate. So we immersed the nanopillar chip in the solutions overnight, and after that, filled and evaporated the solutions in the nanopillar chip three to five times.

The nanospheres were diluted 10,000-fold in deionized water (~18 MΩ·cm) and sonicated for more than 10 min to break up aggregates and then applied to the reservoir. The water droplet containing nanospheres was put on one of the reservoirs and then was automatically introduced into the channel and the nanopillar region by capillary action. After the introduction of water was confirmed by an optical microscope, the single-particle tracking experiment was begun. The washing method mentioned above was applied to discharge the water from the channel and the nanopillar region. Single-particle trajectories were observed using a 100-W mercury arc lamp-illuminated inverted fluorescence microscope (Axiovert 135TV, Carl Zeiss, Tokyo, Japan) thorough a 100x/1.3 NA objective (Carl Zeiss). Brownian motion of nanospheres was captured by video-rate CCD camera (C7190-43, Hamamatsu Photonics, Hamamatsu, Japan), recorded on DV tape (DSR-11, SONY, Tokyo, Japan), and transferred to a computer. The centers of mass of fluorescent spots were analyzed and traced with image-processing software (Cosmos32, Library, Tokyo, Japan). All SPT measurement was done at 25 °C.

Table 1 Average diffusion coefficients (n=17) and their standard deviations at four different time intervals

Time intervals (ms)	Channel	Nanopillars
33	3.18±2.96	1.84±1.38
66	3.18±2.92	1.84±1.38
99	3.16±2.88	1.84±1.38
132	3.15±2.84	1.84±1.37

Results and discussion

Calibration of single-particle tracking

Quasi two-dimensional Brownian motion of nanospheres was traced from the sequential video images. The displacement of ith particle at time t, $\Delta x_i(t) = x_i(t) - x_i(0)$ and $\Delta y_i(t) = y_i(t) - y_i(0)$, gives the square displacement according to the following equation:

$$[\Delta R_i(t)]^2 = [\Delta x_i(t)]^2 + [\Delta y_i(t)]^2 \tag{1}$$

To obtain a diffusion coefficient, mean-square displacements $\langle R^2 \rangle$ should be calculated as a function of time:

$$\langle R^2 \rangle = \frac{1}{N}\sum_{i=1}^{N}[\Delta R_i(t)]^2 \tag{2}$$

where N is the total number of frames that have been traced (over 600 frames in this case). When the nanospheres undergo normal diffusion, the slope of the $\langle R^2 \rangle - \Delta t$ plot should be linear and $\langle R^2 \rangle$ can be expressed as follows:

$$\langle R_x^2 \rangle = 2D_x t \quad \langle R_y^2 \rangle = 2D_y t \tag{3}$$

$$\langle R^2 \rangle = \langle R_x^2 \rangle + \langle R_y^2 \rangle \tag{4}$$

$$2D_x t + 2D_y t = 4Dt \tag{5}$$

where D is the two-dimensional diffusion coefficient and D_x and D_y are one-dimensional diffusion coefficients for the x and y directions, respectively. Therefore, we could calculate the diffusion coefficient from the slope of the plot of $\langle R^2 \rangle - \Delta t$. While the diffusion coefficient can be obtained experimentally as mentioned above, the Stokes-Einstein equation also provides the diffusion coefficient of

a small particle based on thermodynamic and hydrodynamic views on diffusion. The equation is given by:

$$D = \frac{k_B T}{6\pi\eta r} \tag{6}$$

where k_B is Boltzmann's constant, T is the absolute temperature, η is the viscosity of the fluid and r is the radius of the diffusing particle. Comparing the diffusion coefficients obtained from Eqs. (5) and (6), we can estimate the differences in viscosity between bulk space and nanospace.

In membrane dynamic studies using SPT technique, as Kusumi et al. mentioned [18], the diffusion coefficient determined by SPT could provide the diffusion rate within membrane compartments that are only submicrometer-sized. Thus the authors refer to the diffusion coefficient estimated from SPT as the "microscopic" diffusion coefficient. In contrast, what we would like to investigate is the viscosity of water in nanospace based on the diffusion coefficient. It is the interactions between the nanospheres and the surrounding water that should be examined, not the nanospheres or the surfaces of the channel and the nanopillars. To prevent this, a lower concentration of nanospheres should be used for SPT measurement in the shortest possible time. In our microscopic observation system, the images were taken every 33 ms at 640×480-pixel resolution, with one pixel square being nearly equivalent to 120 nm^2. Considering the channel height (400 nm) and the spaces between nanopillars (500 nm), in order to validate SPT technique, a diffusion coefficient was first calculated by fitting the $\langle R^2 \rangle$ at time intervals of 33, 66, 99 and 132 ms over the whole observation time (20–30 s). The results are shown in Table 1. Differences between the means of the diffusion coefficients at each time interval were assessed with t-test. The diffusion coefficients did not change significantly in these time intervals. The averaged diffusion coefficients and their standard deviations show no significant differences among these time intervals. Though longer trajectory measurements are preferable to reduce the statistical errors yielded in the process of image analysis, trajectory measurements below 400 or 500 nm are preferred to exclude other factors that might influence a nanosphere's motion. Considering these points, diffusion coefficients at 132-ms time intervals were assumed to reflect the actual value.

Diffusion coefficients in nanospace

The diffusion coefficients at 132-ms time intervals were measured for 17 different particles over 20 s, and the diffusion coefficients of D_{channel}=3.15 μm^2/s in the nanochannels and $D_{\text{nanopillars}}$=1.84 μm^2/s in the nanopillars were obtained from the slope. These values could not be simply compared because geometrical differences, especially the area occupied by the 500-nm wide nanopillar itself and a difference in the interfacial area ratios, were not factors in the calculation. Although there was little difference between the interfacial area ratio in the nanochannel and the nanopillars (50×50 μm region, 5,040 μm^2/1,000 μm^3 in the nanochannel and 5,630 μm^2/1,000 μm^3 in the nanopillars), the degrees of freedom of possible trajectory in the nanopillars are obviously lower than in the nanochannels. Despite the differences in the degrees of freedom, we calculated the diffusion coefficients on the assumption that the nanopillars have zero volume but the same electrostatic properties as quartz.

Diffusion coefficients could be also estimated from Eq. (6), and the calculated value was D_{theory}=9.81 μm^2/s at 25 °C. Even if we could not simply compare the D_{channel} with the $D_{\text{nanopillars}}$, both of them are obviously smaller than the D_{theory}. The smaller diffusion coefficient suggested higher viscosity in the nanometer-high channels and the nanopillars. In keeping with the suggestions of Hibara et al. in their liquid introduction experiment [15], our SPT measurement also suggested that the viscosity of the liquid became higher in nanospace.

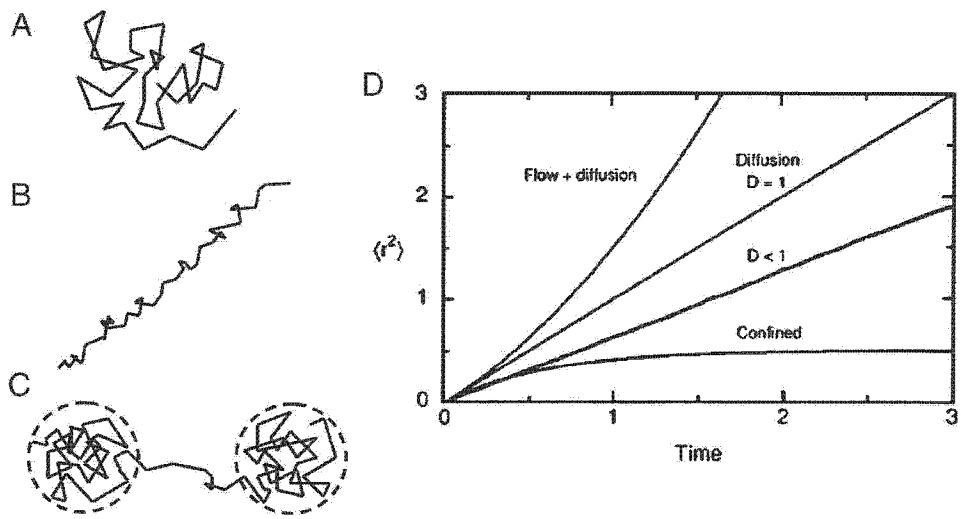

Fig. 2 Diagram of typical trajectories of different modes of motion: **a** simple diffusion, **b** directed motion, e.g., flowing beads under a hydrodynamic flow, and **c** confined motion, e.g., membrane proteins on the cell surface. **d** The relationship between the mean-square displacement $\langle r^2 \rangle$ and time t under various diffusion motions. This figure was reprinted, with permission, from the Annual Review of Biomolecular Structure, Volume 26 (c) 1997 by Annual Reviews http://www.annualreviews.org

Classification of modes of motion

While the SPT measurement over a short time period reflects a diffusion coefficient in microscopic surroundings, a long-time trajectory measurement over a few seconds gives several modes of motion of individual molecules: immobile, directed, confined, tethered, normal diffusion, and anomalous diffusion (Fig. 2) [16–18]. In the present study, the long-time observation of nanosphere motions and a classification of their motions would suggest the presence of a hydrodynamic flow under a geometrical confinement. Due to the simple geometry of the nanochannel and the nanopillars, the motions of nanospheres are expected to be classified into fewer modes than those observed in membrane dynamic studies. The main objective in this study was to investigate liquid properties in nanospace as well as the presence of a hydrodynamic flow in the nanochannel. In a microchip electrophoresis system without using polymer matrices, a difference in fluid level between the reservoirs generates a hydrodynamic flow and affects the resolution or the reproducibility of the separation. Nano-sized channels or nano-sized pillars, which had been suggested to increase the microscopic liquid viscosity, were expected to hold liquids tightly in their structures and prevent a hydrodynamic flow. In our previous study on DNA separation using nanopillar chips [19], it was practically impossible to detect a hydrodynamic flow in the nanopillar chips during DNA separation.

In this study, we classified the motion of nanospheres into the following three modes: simple diffusion, directed diffu-

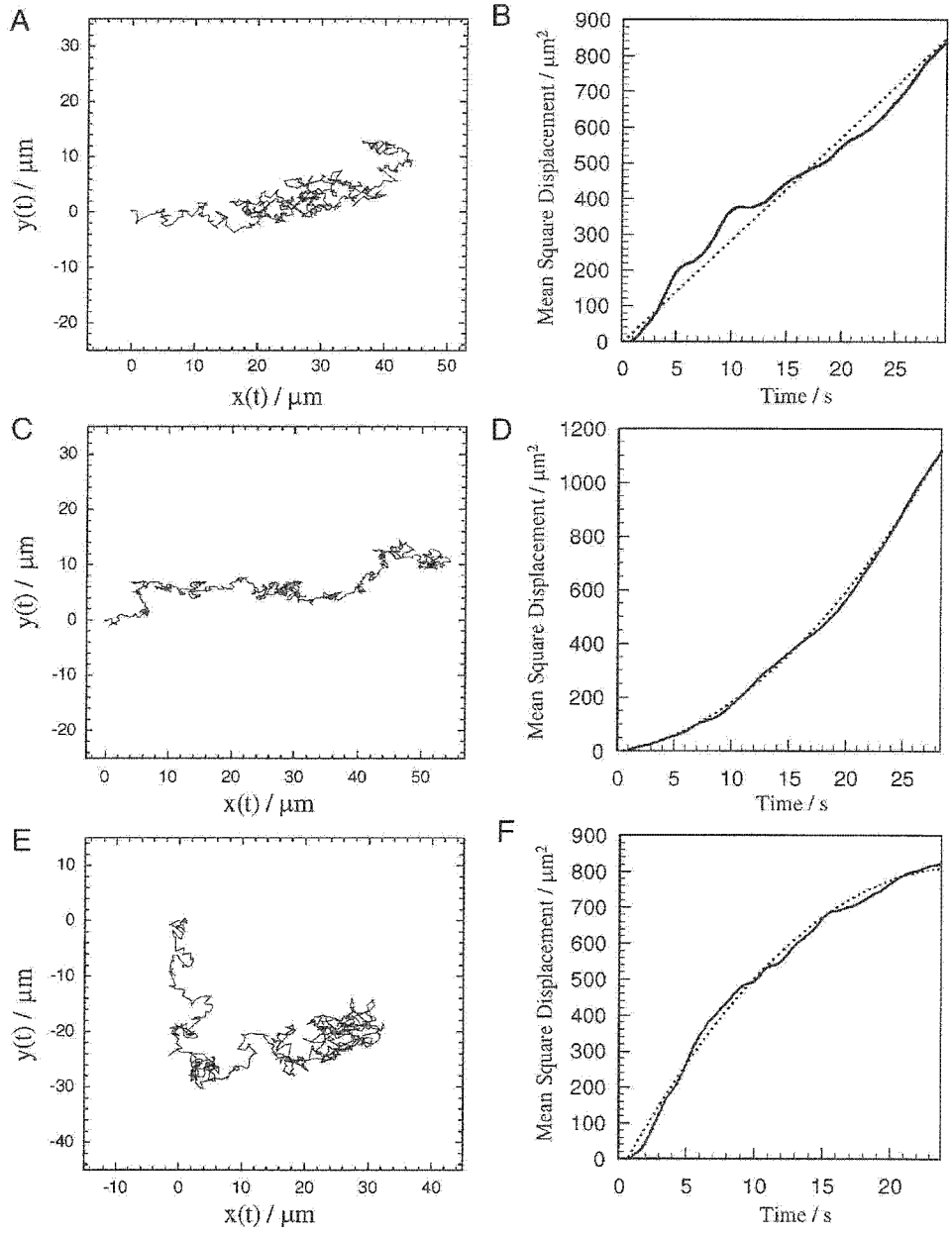

Fig. 3 Typical trajectories of nanospheres (**a**, **c**, **e**) and the corresponding plots (**b**, **d**, **f**). Based on the result of least-square fitting, plots were classified into three modes of motion: **b** simple diffusion, **d** directed diffusion, and **f** others

Table 2 The number of classified nanospheres with the percentage of total amount *in parentheses*

	Channel	Nanopillars
Simple diffusion	7 (41%)	9 (53%)
Directed diffusion	7 (41%)	4 (24%)
Others	3 (18%)	4 (24%)

sion, which implies the presence of hydrodynamic flow, and others. Fitting of $\langle R^2 \rangle - \Delta t$ was carried out by Levenberg-Marquardt method, and motions were classified based on the correlation factors. Figure 3 shows a typical trajectory of the nanospheres and their $\langle R^2 \rangle - \Delta t$ plot. These representative trajectories were drawn by connecting the positions of the nanospheres from the sequential video images. Though the trajectories were complex, the $\langle R^2 \rangle - \Delta t$ plot showed distinct differences among the modes. A total of 34 nanobeads, in the channel and the nanopillars, were analyzed to classify the motions. Consequently, as shown in Table 2, more directed diffusion was observed in the nanochannel than in the nanopillars. This result indicates that the nanopillars prevent a hydrodynamic flow to some extent even when the adjacent nanochannel has a hydrodynamic flow. Of course the nanopillars were not fully able to prevent the hydrodynamic flow, but relatively speaking, the degree of hydrodynamic flow was smaller than that in the channel. The low reproducibility of the DNA migration time in our previous work could possibly be attributed to the hydrodynamic flow or the different degrees of hydrodynamic flow in the channel and the nanopillars. The coexistence of a different degree of hydrodynamic flow in the nanopillar chips should be considered as one factor for achieving high-resolution DNA separation with an excellent reproducibility.

Acknowledgements The present work was partially supported by a Grant from New Energy and Industrial Technology Development Organization (NEDO) of the Ministry of Economy and a Grant-in-Aid for Scientific Research from the Ministry of Education, Science and Technology, Japan.

References

1. Turner SW, Cabodi M, Craighead HG (2002) Phys Rev Lett 88:128103
2. Han J, Turner SW, Craighead HG (1999) Phys Rev Lett 83:1688–1691
3. Han J, Craighead HG (2002) Anal Chem 74:394–401
4. Han J, Craighead HG (2000) Science 288:1026–1029
5. Cabodi M, Turner SW, Craighead HG (2002) Anal Chem 74:5169–5174
6. Tas NR, Mela P, Kramer T, Berenschot JW, van den Berg A (2003) Nano Lett 3:1537–1540
7. Pu Q, Yun J, Temkin H, Liu S (2004) Nano Lett 4:1099–1103
8. Liu S, Pu Q, Gao L, Korzeniewski C, Matzke C (2005) Nano Lett 5:1389–1393
9. Tsukahara T, Hibara A, Kitamori T (2005) Proc μTAS 2005:1255–1257
10. Tsukahara T, Hibara A, Kitamori T (2004) Proc μTAS 2004:189–191
11. Hibara A, Saito T, Kim HB, Tokeshi M, Ooi T, Nakao M, Kitamori T (2002) Anal Chem 74:6170–6176
12. Ohba T, Kanoh H, Kaneko K (2005) Nano Lett 5:227–230
13. Naguib N, Ye H, Gogotsi Y, Yazicioglu AG, Megaridis CM, Yoshimura M (2004) Nano Lett 4:2237–2243
14. Mashl RJ, Joseph S, Aluru NR, Jakobsson E (2003) Nano Lett 3:589–592
15. Xu XH, Yeung ES (1997) Science 275:1106–1109
16. Saxton MJ, Jacobson K (1997) Annu Rev Biophys Biomol Struct 26:373–399
17. Qian H, Sheetz MP, Elson EL (1991) Biophys J 60:910–921
18. Kusumi A, Sako Y, Yamamoto M (1993) Biophys J 65:2021–2040
19. Kaji N, Tezuka Y, Takamura Y, Ueda M, Nishimoto T, Nakanishi H, Horiike Y, Baba Y (2004) Anal Chem 76:15–22

ナノテクノロジーとバイオセンサ

各論 Ⅲ. マイクロチップ分析関連

3. 無痛針による微量採血分析から在宅で健康診断できるヘルスケアチップの開発

堀池 靖浩　甲田 裕子　小川 洋輝　長井 政雄

臨 床 検 査

第50巻 第12号 増刊号 別刷

2006年11月30日 発行

医学書院

各論 Ⅲ．マイクロチップ分析関連

3．無痛針による微量採血分析から在宅で健康診断できるヘルスケアチップの開発

堀池靖浩[1)]/甲田裕子/小川洋輝[2)]/長井政雄

〔KEYWORDS〕 無痛針，在宅診断，μTAS，ヘルスケアチップ，電気化学法，比色法

はじめに

わが国では近年，少子高齢化が進行し，高齢者が占める医療費のコストの激増が国家予算を圧迫するとともに，少子化による労働力の不足により国力を衰退させることが危惧される．この包括的解決の一策は，高齢者が働く意欲のある限り働き，培った知恵と経験を社会に還元できるよう元気で毎日を送れる「健康立国」を世界に先駆けわが国に創り出すことである．このためには予防が大切であり，簡便・迅速なバイオセンシング技術を早急に確立しなければならない．一方，μTAS (micro total analytical system)やLab on a Chip[1)]と呼ばれる小面積の基板に異なった分析部品を機能的に集積化して微量試料を分析する新研究分野が近年急激に発展し，その出口の1つとして種々のバイオチップの出現が期待されている．筆者らはその一貫として，微量の採血から在宅で簡便・確実に同時多項目を診断できる種々の診断用POCT(point-of-care testing)チップを開発している．図1にバイオチップ開発の目的とその展開をまとめたが，種々の診断チップが整うと，計測された多項目のマーカー値を医療施設に通信回線で送り，医療ブロードバンドネットワークと高精細ディスプレイを介して医師による問診が在宅で可能になる．検出マーカーを増やし，長期間の使用によって，医療施設に多数の方の健康・疾病マーカーの推移が蓄積されたデータベースが構築され，そのマーカーと疾病との相関関係を解明が可能になる．さらには，医師不在の寒村や離島の人々の遠隔診断が実現される．

本稿では，まず現在商用の各種POCT生化学分析装置を紹介し，筆者らの在宅検査を目指した無痛針から採取した微量の血液の電気化学法[2)]や比色法[3,4)]による分析によって健康・疾病マーカーを測定するヘルスケアチップを解説する．これらのバイオチップの製作については拙著[5)]に譲り，言及しない．

各種POCT生化学分析装置の現状

血液採取に基づくPOCT生化学分析装置として，現在，数社から血液の診断に基づいたバイオチップが実用化されている．ランセットと呼ばれる瞬間に指先を穿刺，採血し，血糖値の1項目だけ調べる血糖値モニターは，国内外とも多く販売され，糖尿病患者のPOCTに貢献している．一方，バイオチップとしては，米国のBiosite Triage Cardiac system[6)]は，マイクロ流路を基にしたデバイスを用いて全血から心臓病マーカーをPOC測定する．Micronics Inc.の「ORCAマイクロ流路プラットフォーム」は，拡散を基本にしたHフィルターやT-センサーなどのような種々の圧力駆動型マイクロ流体力学の要素部品を

1）HORIIKE Yasuhiro, KODA Hiroko　独立行政法人　物質・材料研究機構
2）OGAWA Hiroki, NAGAI Masao　アドビック(株)